LASER & PHOTONICS REVIEWS
www.lpr-journal.org

Toward Laser-Driven Lighting with High Overall Optical Performance: Thermally Robust Composite Phosphor-in-Glass Film

Zezhong Yang, Song Zheng, Sifan Zhuo, Shisheng Lin, Tao Pang, Lingwei Zeng, Jing Wang,* Ping Lu,* Feng Huang, and Daqin Chen**

For laser-driven white light sources, phosphor-in-glass films (PiGFs), typically sintered onto substrates with high-thermal conductivity, are developed and emerged as the leading materials. However, compared to other all-inorganic color converters, such as single crystals, transparent ceramics, PiGF suffers from a low saturation threshold, poor thermal stability and limited irradiation durability, which restricts its practical applications. To overcome these limitations, in this study, a series of h-BN-YAG:Ce^{3+} PiGF is developed on opaque Al_2O_3/transparent Al_2O_3 (B-Y PiGF@o/t-Al_2O_3) by directly incorporating high-thermal-conductivity fillers into the PiGF. The selective incorporation of h-BN establishes a local heat conduction network, significantly increasing the saturation threshold and luminous flux. Through optimization, a maximum luminous flux of 6015.46 ± 14.46 lm with a saturation threshold of 16.15 ± 0.48 W mm^{-2} is achieved in reflective excitation mode, outperforming previous high-performance PiGFs. The addition of h-BN both enhanced heat dissipation and improved the uniformity of white light output in transmissive excitation mode, addressing the "yellow ring" effect commonly seen in laser-driven lighting. The application potential of the developed composite has been proven ranging from automotive headlights to medical lighting, offering a path toward enhanced brightness, more efficient, and operational-stable next-generation lighting technologies.

1. Introduction

Laser-driven white light sources, combining blue lasers with color converters, offer superior collimation, directionality, and enhanced luminance, which effectively circumvents the "efficiency droop" limitation of traditional white light-emitting diodes (wLEDs).[1–3] With these characteristics, they are ideal for high-power special lighting applications, such as automotive lighting, searchlights, and maritime illumination. Color converters play a crucial role in determining the overall performance of laser-driven white light, placing stringent demands on their luminescence capabilities and thermal management.[4–8] Currently, single crystals (SCs),[9–11] transparent ceramics (TCs),[12–16] phosphor-in-glass (PiGs),[17–20] and PiGFs[21–33] exhibit potential as color converters for laser-driven lighting. Among these, PiGs can be prepared more easily while yielding flexible spectra by the combination of different phosphors. However, the low thermal conductivity of the glass matrix (≈1 W $m^{-1}K^{-1}$) limits its achievable saturation threshold and luminous flux under laser irradiation. In response, phosphor-in-glass films (PiGFs), typically sintered onto substrates with high-thermal conductivity, have been developed and emerged as the leading materials in this field.

For PiGFs, stable performance under high-power blue laser irradiation is crucial, which is influenced by phosphor

Z. Yang, S. Zheng, S. Zhuo, S. Lin, F. Huang, D. Chen
College of Physics and Energy
Fujian Normal University
Fuzhou, Fujian 350117, P. R. China
E-mail: linshisheng@fjnu.edu.cn; dqchen@fjnu.edu.cn

T. Pang
Huzhou Key Laboratory of Materials for Energy Conversion and Storage
College of Science
Huzhou University
Huzhou, Zhejiang 313000, P. R. China

L. Zeng
School of Chemistry and Chemical Engineering
Hunan University of Science and Technology
Xiangtan, Hunan 411201, P. R. China

J. Wang
Ministry of Education Key Laboratory of Bioinorganic and Synthetic Chemistry
State Key Laboratory of Optoelectronic Materials and Technologies
School of Chemistry
Sun Yat-Sen University
Guangzhou, Guangdong 510275, P. R. China
E-mail: ceswj@mail.sysu.edu.cn

P. Lu
School of Materials Science and Engineering
Wuhan University of Technology
Wuhan, Hubei 430070, P. R. China
E-mail: lupingwh@whut.edu.cn

DOI: 10.1002/lpor.202401798

properties (e.g., Stokes shift, luminescence lifetime, thermal stability, and interactions with the glass matrix) and thermal management (primarily through high-thermal-conductivity substrates). An effective thermal management design can enhance the transfer of generated thermal phonons, further reducing thermal ionization and ensuring stable, high-quality white light output.[8,32,33] However, the selection of high-thermal-conductivity substrates has been limited, because it needs to match the thermal expansion coefficients of the substrate and glass to prevent the cracking of the PiGF.[34,35] Therefore, a promising strategy involves directly incorporating high-thermal-conductivity fillers into the PiGF.

In this context, hexagonal boron nitride (h-BN) exhibits a graphene-like honeycomb structure, with atoms bonded by strong covalent interactions. This robust atomic arrangement minimizes phonon scattering within the lattice, resulting in its exceptional in-plane thermal conductivity (up to 400 W $m^{-1}K^{-1}$).[36–38] The incorporation of micrometer-scale BN into $Y_{1.31}Gd_{1.6}Al_5O_{12}$: $0.09Ce^{3+}$ (GdYAG: Ce) PiGF by Xiang et al. significantly increased the saturation threshold from 3.12 to 5.42 W mm^{-2}, along with an increase in luminous flux (LF) from 260.6 to 354.1 lm.[39] Similarly, Xie et al. found that the use of h-BN as a scattering medium in a $(La, Y)_3Si_6N_{11}$: Ce^{3+} (LYSN: Ce) PiGF enhanced both thermal and optical performance, achieving an internal quantum efficiency (IQE) of 70 % and a luminescence saturation threshold of 12.82 W mm^{-2}—both substantially higher than those observed without h-BN.[40] Luo et al. reported that the incorporation of h-BN flakes with quantum dots improved the thermal conductivity of the optical conversion layer by 50 % at a 4.3 wt% h-BN content.[37] Although some researchers have made significant strides in improving the thermal and optical performance of PiGF by incorporating h-BN, limitations still persist, such as insufficient luminous flux, lack of photometric/chromatic controllability, and the neglect of light uniformity. Therefore, further research into these aspects would greatly enhance the potential of PiGFs in various lighting applications.

Herein, we developed a series of h-BN-YAG: Ce^{3+} PiGF on opaque Al_2O_3/transparent Al_2O_3 (sapphire) substrates (abbreviated as B-Y PiGF@o/t-Al_2O_3) composite color converters. In reflective excitation mode, after optimization, the saturation threshold increased to 16.15 W mm^{-2}, with a maximum luminous flux (LF) of 6015.46 ± 14.46 lm, demonstrating superior parameters compared to previously reported high-performance PiGFs (**Table 1**). Here, the h-BN (≈150 nm) establishes a microzone heat conduction network, further enhancing the performance and stability under high-power-density blue laser irradiation. In transmissive excitation mode, the introduction of h-BN generating an appropriate number of pores effectively improved white light output uniformity, addressing the "yellow ring" issue. Moreover, the laser-driven light source (reflective excitation mode) exhibits excellent beam collimation and long-distance illumination, making it suitable for applications such as automotive lighting. With the incorporation of $CaAlSiN_3$: Eu^{2+} (CASN) phosphor, a laser-driven miniature endoscope light source based on the newly developed PiGFs in transmissive excitation mode achieves higher brightness and lower operating temperatures, making it preferable for medical observations compared to LED-based systems.

2. Results and Discussion

2.1. Phase Identification and Microstructure Analysis

B-Y PiGF@Al_2O_3 was synthesized using a straightforward multiple printing-heat treatment method (MPHTM), with the detailed preparation process illustrated in Figure S1 (Supporting Information). The original YAG: Ce^{3+} powders exhibit a well-defined ellipsoidal morphology, with particle sizes ranging from approximately 7–9 µm. In contrast, the h-BN consits of flaky particles with a diameter of approximately 150 nm (Figure S2, Supporting Information). The X-ray diffraction (XRD) pattern of B-Y PiGF@Al_2O_3, depicted in **Figure 1a**, reveals superimposed diffraction patterns (amorphous structure + YAG: Ce^{3+} + h-BN + Al_2O_3). The sharp and intense peaks associated with both YAG: Ce^{3+} and Al_2O_3 closely correspond to the standard cards for YAG: Ce^{3+} (PDF#79-1891) and Al_2O_3 (PDF#34-0421). The diffraction peaks of h-BN are relatively weak due to its low content, and no impurity peaks are detected. SEM-EDS mappings (Figure 1b) demonstrate a distinct boundary between the YAG: Ce^{3+} particles and the glass matrix, indicating the absence of interfacial reactions during the co-sintering process. The SEM images (Figure 1c) further illustrate that the YAG: Ce^{3+} phosphor is tightly encapsulated by the glass matrix, with h-BN primarily adhering closely to the phosphor particles. Based on the previous work, this study enhances the process by incorporating MPHTM for PiGF preparation, facilitating a scalable approach for commercial production. As shown in Figure 1d,e, the film produced via MPHTM exhibits a relatively uniform surface structure and thickness. Notably, with the inclusion of h-BN (150 nm), some pores appear in the B-Y PiGF film, scattering light and homogenizing the white light distribution. However, with high h-BN content (reaching 10 wt%), a significant reduction can be found in film compactness, leading to the susceptibility of film to delamination from the substrate (Figures S3 and S4, Supporting Information).

2.2. Optical Properties

The B-Y PiGF@Al_2O_3 emits bright yellow light under blue light illumination (**Figure 2a**). The photoluminescence (PL) spectrum of B-Y PiGF@Al_2O_3 (Figure 2b) exhibits a broad emission centered at approximately 550 nm, indicative of the Ce^{3+} 5d→4f transition.[12,16] Decay kinetics measurements reveal an almost invariant fluorescence lifetime of approximately 65 ns upon co-sintering (Figure 2c). As depicted in Figure 2d and Figure S5

D. Chen
Fujian Provincial Collaborative Innovation Center for Advanced High-Field Superconducting Materials and Engineering
Fujian Normal University
Fuzhou, Fujian 350117, P. R. China
D. Chen
Fujian Provincial Engineering Technology Research Center of Solar Energy Conversion and Energy Storage
Fujian Normal University
Fuzhou, Fujian 350117, P. R. China

Table 1. The reported optical performance of previous high-performance PiGFs under blue laser excitation in reflective mode.

Sample	Saturation Threshold [W mm^{-2}]	Saturated Luminous Flux [lm]	Luminous Exitance [lm mm^{-2}]	Refs.
$La_3Si_6N_{11}$:Ce^{3+} PiGF@sapphire	5.5	550	550	[24]
$Y_3Al_5O_{12}$:Ce^{3+} PiGF@sapphire	10.5	1350	1350	[26]
$Y_{1.31}Ce_{0.09}Gd_{1.6}Al_5O_{12}$ PiGF@sapphire	5.42	354.1	451	[39]
YAG:Ce, LuAG:Ce, CASN:Eu PiGF@sapphire	9.32	983.2	1983.2	[25]
$Y_3Al_5O_{12}$:Ce^{3+} PiGF@sapphire	8	1300	1656	[21]
$La_3Si_6N_{11}$:Ce^{3+} PiGF@sapphire	6.62	1071.73	1365	[31]
$Y_3(Ga,Al)_5O_{12}$:Ce^{3+} PiGF@sapphire	16	1475.9	1419.13	[22]
This work	16.15	6015.46	2368	

(Supporting Information), after the incorporation of h-BN, the internal quantum efficiency (IQE) of the PiGF consistently surpasses 98 %. With the increased h-BN content, a gradual decline can be observed in absorption efficiency and external quantum efficiency (EQE), attributed to the restricted incident-photon scattering range induced by the pores from coated h-BN. Although a reduction in EQE is typically undesirable, the benefits of enhanced light scattering and thermal management may still dominate in optimizing heat dissipation, optical performance, and system reliability.

Thermal stability represents a critical factor in laser-driven lighting applications.[26,32] We systematically investigated the temperature-dependent PL spectra of PiGFs with varied h-BN content. As illustrated in Figure 2e,f, the relative integrated PL

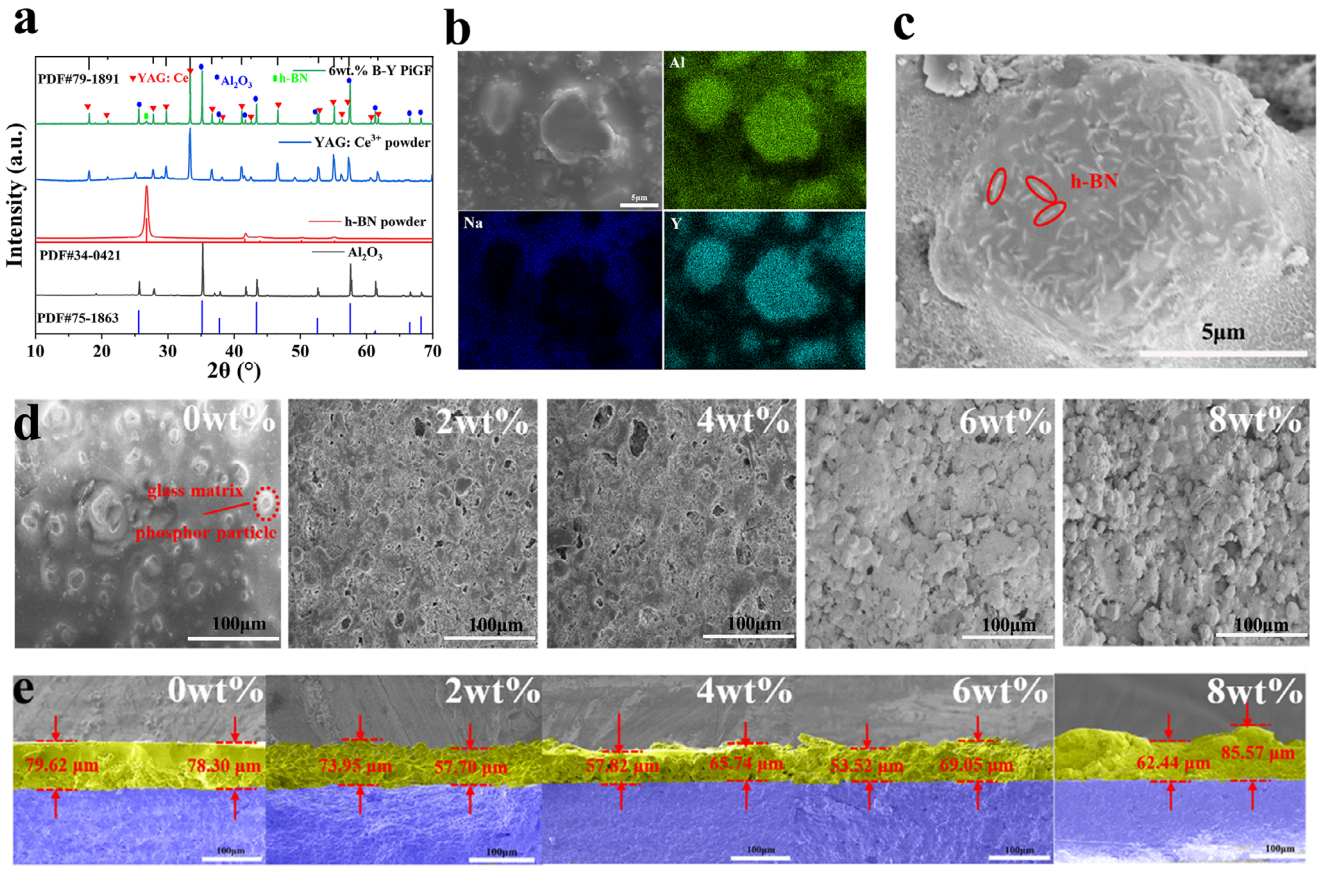

Figure 1. a) XRD patterns of YAG:Ce powder, h-BN powder, Al_2O_3 substrate and B-Y PiGF@Al_2O_3; b) SEM image and the corresponding EDS mappings of B-Y PiGF@Al_2O_3; c) SEM image of the enlarged region of B-Y PiGF@Al_2O_3; SEM images of d) the front surface and e) the side view of B-Y PiGF@Al_2O_3 with varying h-BN content.

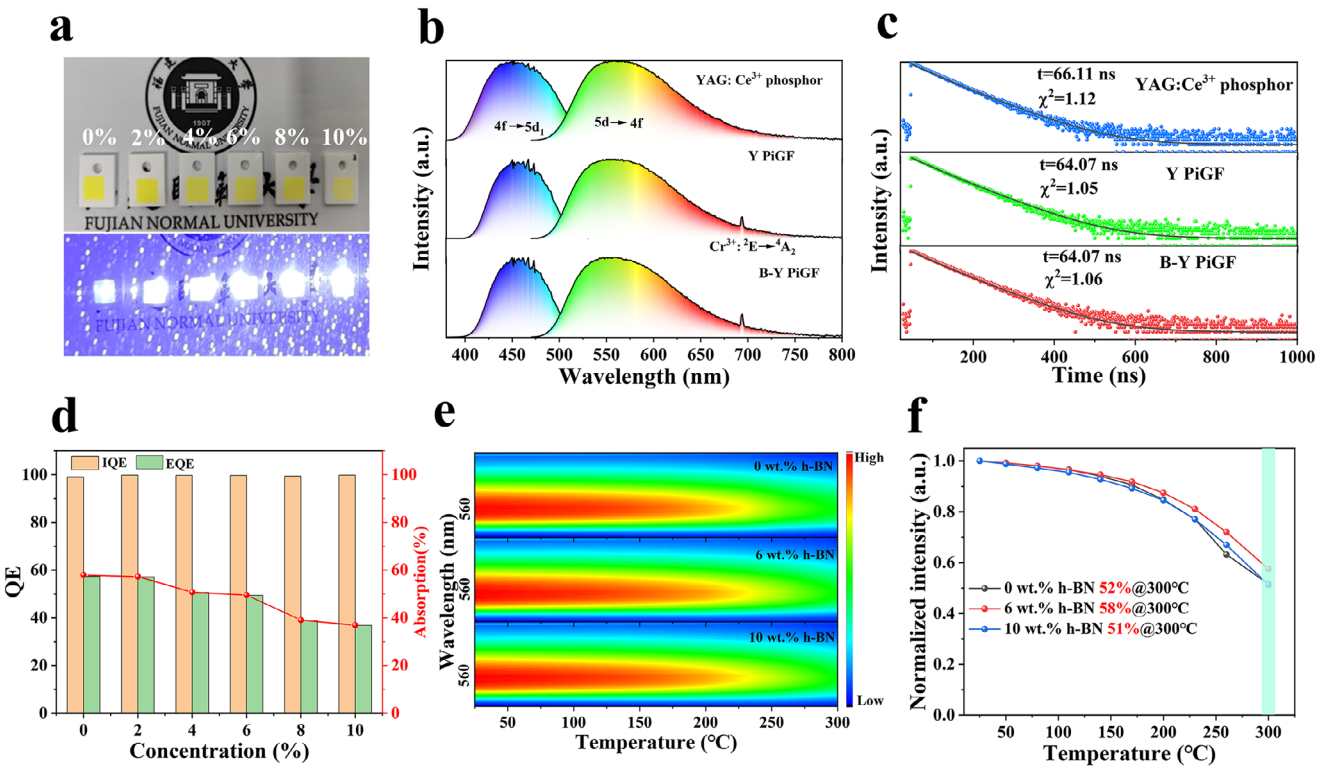

Figure 2. a) Appearance of the B-Y PiGF@Al_2O_3 with varying h-BN contents under daylight and blue laser light irradiation (Note: Fujian Normal University grants permission to use its logo); b) PL, PLE spectra, and c) lifetime decay curves of original YAG:Ce^{3+} phosphor, Y PiGF, and B-Y PiGF; d) IQE, EQE and absorption characteristics of B-Y PiGF with different h-BN contents; e) Contour plots of the emission spectra and f) normalized change curves collected as a function of temperature ranging from 25 to 300 °C.

intensity of PiGF containing 0 wt%, 6 wt%, and 10 wt% h-BN consistently declines with elevation of temperature, due to thermally assisted non-radiative transitions. The integrated PL intensity for 0 wt%, 6 wt%, and 10 wt% B-Y PiGF remains above 80% at 200 °C compared to its value at 25 °C, indicating that the co-sintering process does not affect the thermally robustness and ruling out structural damage as the cause for the EQE decrease. Notably, as the temperature exceeds 200 °C, 6 wt% B-Y PiGFs demonstrate superior thermal stability compared to 0 wt% B-Y PiGFs, attributed to the high thermal conductivity of h-BN. However, as the h-BN content increases to 10 wt%, the loose structural compactness of the 10 wt% B-Y PiGFs leads to a degradation in thermal quenching performance. For instance, the luminescent losses for 0 wt%, 6 wt%, and 10 wt% B-Y PiGFs are approximately 48 %, 42 %, and 49 % at 573 K (300 °C), respectively.

2.3. Luminescent Behaviors Under Blue Laser Irradiation

2.3.1. Reflective Excitation Mode

First, in order to evaluate the luminescent performance of samples modified with h-BN of varying sizes, a simple comparison was conducted utilizing a self-built laser-driven lighting testing device (Figure S6, Supporting Information). It was observed that samples containing h-BN particles with a size of 150 nm exhibited superior performance, as larger h-BN particles are not conducive to heat dissipation from the phosphors to the surrounding environment (Figure S7, Supporting Information). This research consistently utilizes h-BN with a particle size of 150 nm, unless otherwise specified. In the field of laser-driven lighting, two optical path modes exist: reflection and transmission. The reflectance affects the luminescence properties in reflection mode. The reflectance spectra of 0–10% h-BN PiGF@o-Al_2O_3 have been measured, demonstrating approximately 80% reflectance within the visible light range. A slight increase in reflectance is observed with higher h-BN content (Figure S8, Supporting Information). In the reflective excitation mode, the relationship between the luminous flux of B-Y PiGF@ opaque Al_2O_3 (o-Al_2O_3) and h-BN content was systematically analyzed under increased power-density blue laser irradiation. The 0 wt% B-Y PiGF exhibited a saturation threshold of 7.48 ± 0.22 W mm^{-2} and a luminous flux of 3133.85 ± 11.20 lm (**Figure** 3a–c). In comparison, the 6 wt% B-Y PiGF (with a same thickness of 2 layers) demonstrated a maximum saturation threshold of 14.57 ± 0.44 W mm^{-2}, accompanied by a luminous flux (LF) of 4429.11 ± 4.35 lm, corresponding to enhancements of 95 % and 41 %, respectively. However, since insufficient compactness resulted in a sharp decline in optical performance under high power-density blue laser irradiation, the 10 wt% B-Y PiGF displayed the low saturation threshold of 6.30 W mm^{-2}. The anomalous regularity observed in the 4% h-BN sample is hard to explain and warrants further investigation (Figure 3b). We hypothesize that this phenomenon may stem from a combination of factors, including pore

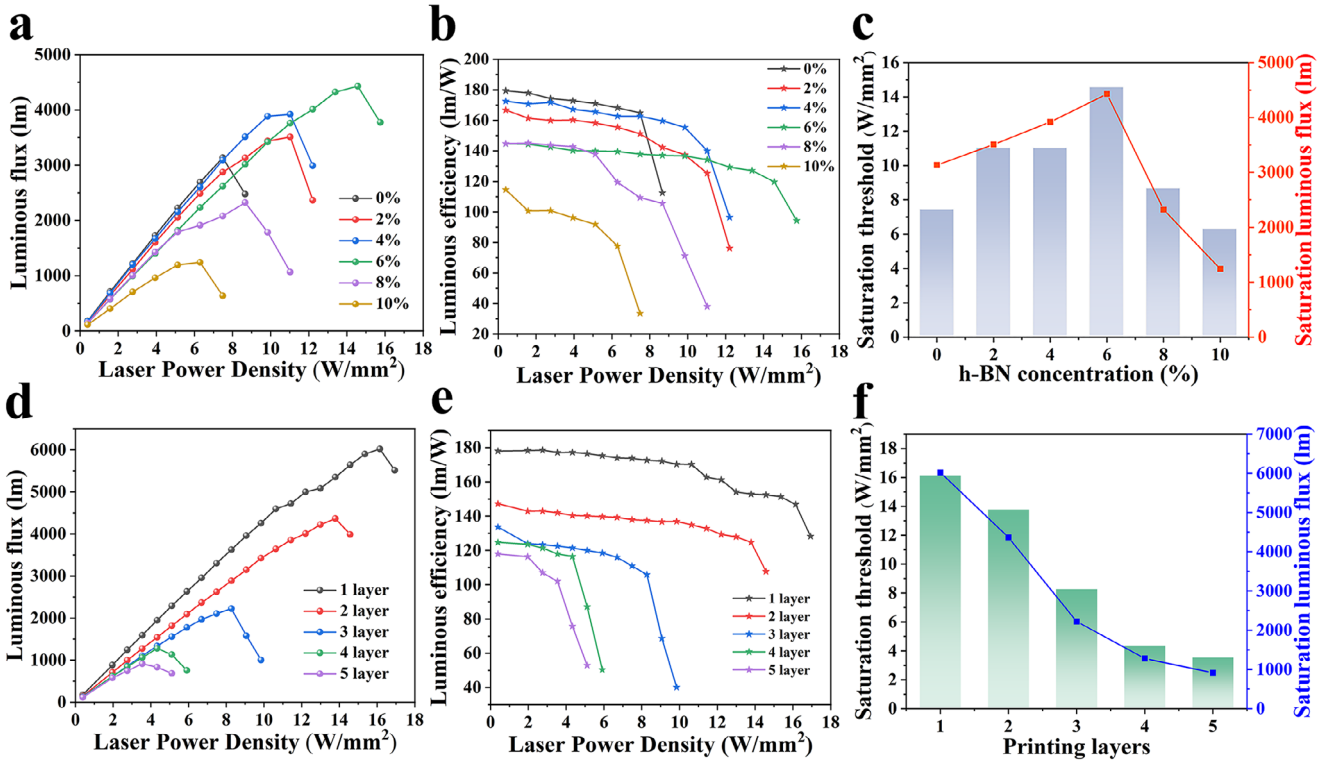

Figure 3. a) Luminous flux, b) luminous efficiency, and c) saturation threshold of B-Y PiGF@Al_2O_3 with varying h-BN content; d) Luminous flux, e) luminous efficiency, and f) saturation threshold of 6 wt% h-BN PiGF with different printing layers.

content, thermal conductivity, and the adhesion quality between the PiG film and the Al_2O_3 substrate. Further analysis reveals that the thickness of PiGF also had a significant impact on luminous flux (Figure 3d–f). Specifically, the sample with 1 layer achieved a maximum saturation threshold of 16.15 ± 0.48 W mm^{-2} and a luminous flux of 6015.46 ± 14.46 lm for the 6 wt% B-Y PiGF. Conversely, the sample with 5 layers exhibited a reduced saturation threshold of 3.54 ± 0.11 W mm^{-2} and a luminous flux of 916.54 ± 4.55 lm, primarily because the increased film thickness caused greater heat accumulation. Evidently, for reflective excitation mode, the optimal h-BN content and PiGF thickness were determined to be 6 wt% and 1 layer, respectively. The saturation luminous flux and luminous exitance of high-performance PiGFs are summarized (Table 1; Figure S9, Supporting Information) for comparative analysis. YAG: Ce^{3+} PiGF@o-Al_2O_3, modified with h-BN (150 nm), achieved a maximum luminous exitance of 2368 lm mm^{-2}, surpassing the majority of related PiGF composites. For each h-BN concentration and PiGF thickness, four independent PiGF samples were prepared under identical conditions to ensure reproducibility (as shown in Tables S1–S4, Supporting Information). Furthermore, the standard deviations of these parameters were calculated across the four samples as a function of increasing power density, with values remaining below 15 lm (Equation S1, Tables S5 and S6, Supporting Information). These analyses confirm the statistical significance of the results, effectively ruling out the possibility of a coincidental outcome.

Based on electroluminescence (EL) spectra, the proportions of blue light and converted light power were calculated, revealing a gradual decrease in the proportion of converted light power with increasing h-BN content (**Figure** 4a), consistent with changes in absorption efficiency (Figure 2d). Consequently, with the increased h-BN content, the correlated color temperature (CCT) of B-Y PiGF progressively rises, reaching 6787 K for 6 wt% B-Y PiGF, with a color rendering index (Ra) of 68.4 (Figure 4b). Ensuring efficient and stable output has been a primary focus of research on laser-driven lighting. As illustrated in Figure 4c, stability tests were conducted: 0 wt% B-Y PiGF@o-Al_2O_3 sample retained only 8% of its initial luminescence performance after 120 min of exposure to irradiation at a power density of 7.48 W mm^{-2} (Figure S10a, Supporting Information), whereas the 6 wt% B-Y PiGF@o-Al_2O_3 maintained an impressive 82 % of its initial performance under the same conditions (Figure S10b, Supporting Information). This significant improvement underscores the beneficial role of selectively incorporating h-BN in enhancing stability and luminescence performance during prolonged lighting. When samples were excited under the same laser power density of 7.48 W mm^{-2}, the local temperature at the spot dramatically decreased from 216.6 °C (0 wt% B-Y PiGF) to 118.8 °C (6 wt% B-Y PiGF) (Figure 4d). Evidently, the addition of h-BN enhances heat dissipation and reduces thermal quenching effects, further facilitating superior thermal management (Figure S11, Supporting Information). Figure 4e depicts the mechanism of enhanced performance through the incorporation of h-BN (150 nm) into YAG: Ce^{3+} PiGF. Typically, when the blue laser irradiates, each phosphor particle acts as a heat source. Since the vast majority of h-BN is firmly attached to the phosphor surface, the generated heat can be efficiently dissipated through the

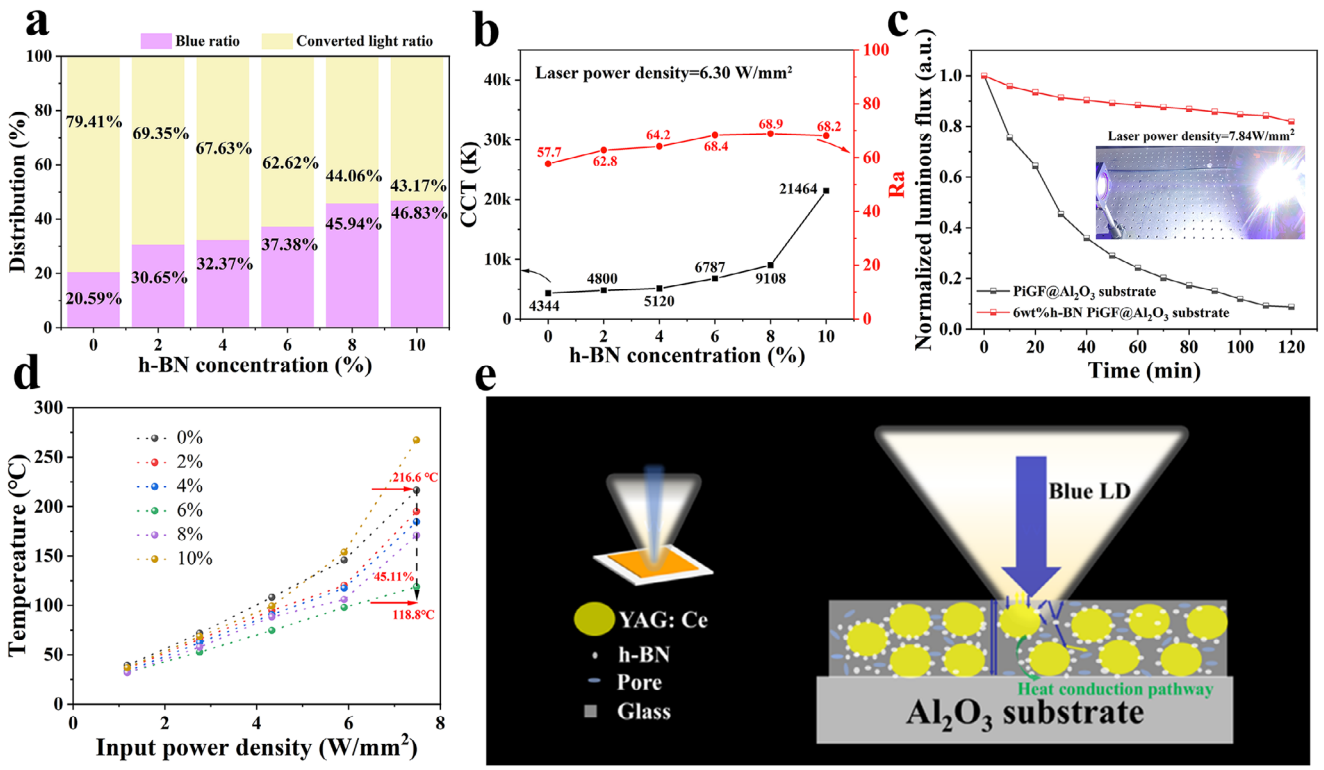

Figure 4. a) Relationship between the ratio of blue light and converted light and h-BN content (2 layers); b) CCT and CRI of samples (2 layers) with varying h-BN content under 6.30 W mm^{-2} blue laser irradiation; c) Comparision of long-term assessments between samples with and without h-BN (2 layers) under a laser power density of 7.48 W mm^{-2}; d) Heat dissipation performance of B-Y PiGF@o-Al_2O_3 with different h-BN contents (2 layers); e) The mechanism of enhanced performance through the incorporation of h-BN into YAG: Ce^{3+} PiGF.

h-BN-forming channels, thus elevating the luminescence performance of the composites under blue laser excitation.[40]

2.3.2. Transmissive Excitation Mode

In the transmissive excitation mode, a prevalent challenge is the occurrence of the "yellow ring" effect, characterized by a central area exhibiting a higher correlated color temperature (CCT). This issue often necessitates intricate optical designs to solve, substantially elevating costs. By integrating h-BN (150 nm) and employing sapphire (transparent Al_2O_3, abbreviated as t-Al_2O_3) as a substrate, the B-Y PiGF@t-Al_2O_3 demonstrated superior optical uniformity compared to commercial YAG: Ce^{3+} PiGF (**Figure 5**a,b). We subsequently measured the transmittance of these samples and noted a gradual decline with the increased phosphor concentration and film thickness (Figure S12, Supporting Information). In transmission mode, the Y2G5-1 layer sample exhibits the highest saturation threshold of 11.68 ± 0.35 W mm^{-2}, achieving a maximum luminous flux of 3195.57 lm (Figure S13, Supporting Information). Formed by the incorporation of h-BN, the pores act as a scattering centers within the PiGF, effectively mitigating blue light leakage and enhancing the overall light uniformity, further resulting in a consistent CCT across various angles (20°-160°) (Figure 5c; Figure S14, Supporting Information). Except for CCT, the spectral analysis reveals remarkable similarities at different angles, further demonstrating that the integration of h-BN substantially enhances the optical uniformity and light-scattering characteristics of the films (Figure S15, Supporting Information). The elevated central color temperature of the sample with the Y1G5-1 layer is attributed to the insufficient phosphor content and inadequate thickness. To be noted, due to the insufficient thickness and low phosphor content of the Y1G5-1 layer PiGF, blue light passes through the film without undergoing adequate scattering, absorption, and conversion, leading to a higher CCT at the center (Figure S16, Supporting Information). Nevertheless, it still outperforms the commercial PiGF in terms of light-uniform performance, as shown in Figure 5a,b. Our investigations further revealed that precise control of CCT and chromaticity coordinates can be achieved by adjusting weight ratio (YtG) and film thickness, thus accommodating broad application requirements. The samples can attain CCTs ranging from 3810 to 8082 K (Figure 5d). The 8082 K color temperature value is also attributable to the insufficient number of color-converter components in the blue laser irradiation area. The precise tuning from cool to neutral white light has been successfully accomplished, showcasing significant potential for diverse lighting applications (Figure 5e).

2.4. Demonstration Experiments

In the reflective excitation mode, we employed the beam-splitting reflection principle to construct a laser-driven white light source

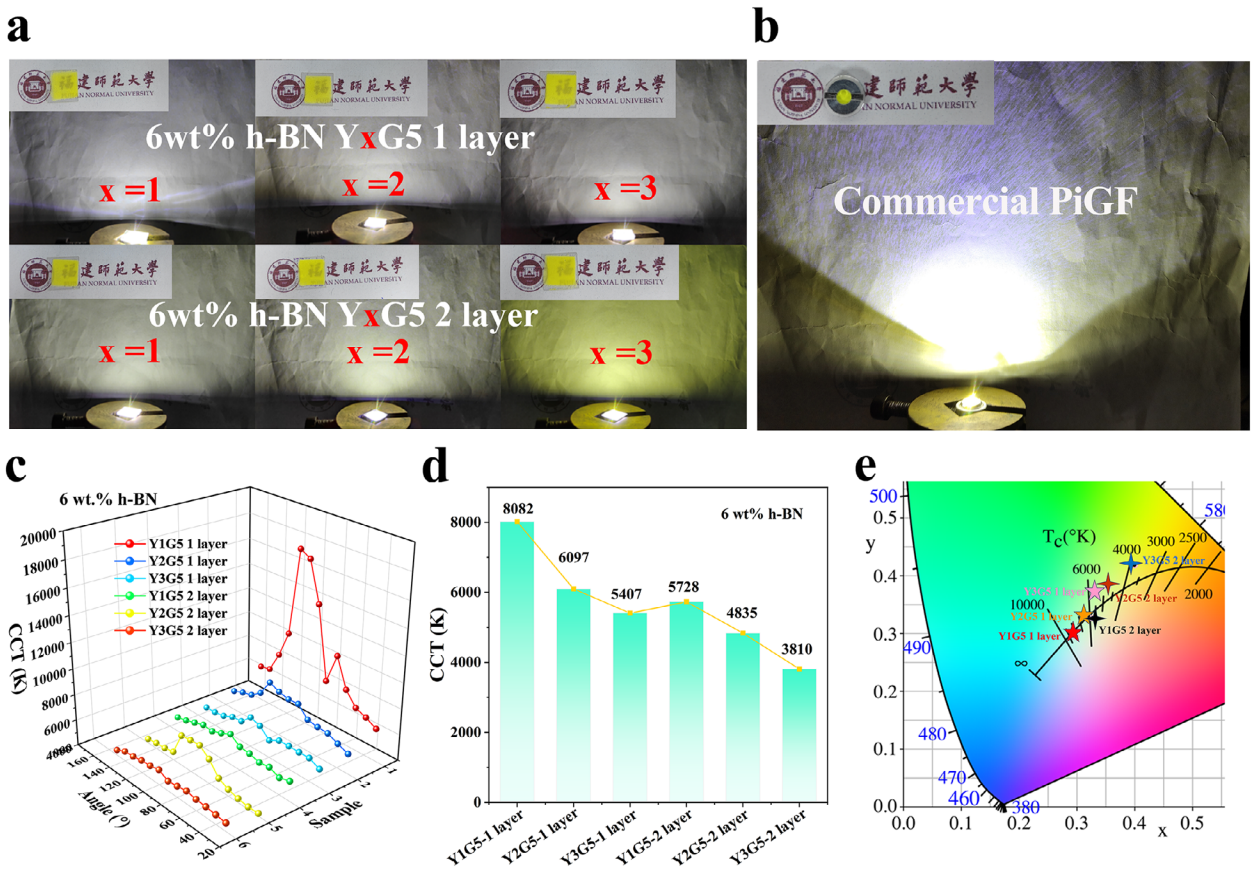

Figure 5. Photographs of a) samples with different YtG ratios and numbers of printed layers under blue laser excitation, and b) commercial YAG: Ce^{3+} PiGF. c) CCT values of B-Y PiGF@t-Al_2O_3 measured at different angles under blue laser excitation (Note: Fujian Normal University grants permission to use its logo). d) CCT and e) chromaticity coordinates of B-Y PiGF@t-Al_2O_3 with different YtG ratios and numbers of printed layers.

(**Figure** 6a). The blue laser beam first passed through a beam splitter, where one part was focused onto the YAG: Ce^{3+} PiGF@o-Al_2O_3 via a lens to generate converted light, while the other reached the reflection module. The reflected blue laser and the converted yellow light were collimated into beams with a low divergence angle through a lens, then combined to produce white light. Experimental validation confirmed the excellent collimation ability of the fabricated light source (Figure 6b; Figure S17, Supporting Information). In the evening, the directional white light could illuminate a building up to 600 m away. The illuminance distance can serve as a valuable indicator for specific application scenarios, such as automotive lighting. In this context, a distance of 600 meters is typically sufficient to allow the driver to respond in a timely manner. However, measuring illuminance at this distance presents challenges due to the large light spot (≈314 mm^2).

In transmittance mode, laser-driven lighting is considered to be explored for miniature endoscope applications; however, the absence of red emission in YAG: Ce^{3+} phosphor limits its color rendering index. Therefore, a series of $CaAlSiN_3$: Eu^{2+} (CASN)-B-Y PiGF@t-Al_2O_3 composites (Figure S18, Supporting Information) were designed with varying CASN/YAG mass ratios (from 0 to 0.20). As the CASN content increased, the EL spectra showed an enhanced red emission relative to yellow (Figure 6c). Correspondingly, the color rendering index (CRI) of $CaAlSiN_3$: Eu^{2+} (CASN)-B-Y PiGF@t-Al_2O_3 gradually increased from 63.3 to 74.0 (Figure 6d). We subsequently fabricated a prototype laser-driven miniature endoscope light source, consisting of a blue laser, CASN-B-Y PiGF@t-Al_2O_3, optical fiber, and a camera module (Figure 6e,f). Under identical input electric power, the laser-driven miniature endoscope demonstrated higher brightness when an object was illuminated on the opposite side of a 1-meter box compared to commercial LED miniature endoscope (Figures S19 and S20, Supporting Information). The temperature at the optical output port was measured for the safety during prolonged operation. The use of an optical fiber allows the highly directional laser-driven white light to be transmitted remotely to the target, resulting in a lower operating temperature. After 30 min of continuous operation, the temperature at the light outlet of the laser-driven miniature endoscope only reached 24.2 °C (Figure S20, Supporting Information). In contrast, with the LED-based endoscope, where the surface-emitting LED is located at the optical output port, local heat accumulation occurred, reaching 53.6 °C, which is not ideal for the prolonged observation of tissues and organs. The local heat accumulation observed in the LED-based endoscope is related to the structural design of the endoscope, particularly the placement of the surface-emitting LEDs at the optical output port. However, it is important to note

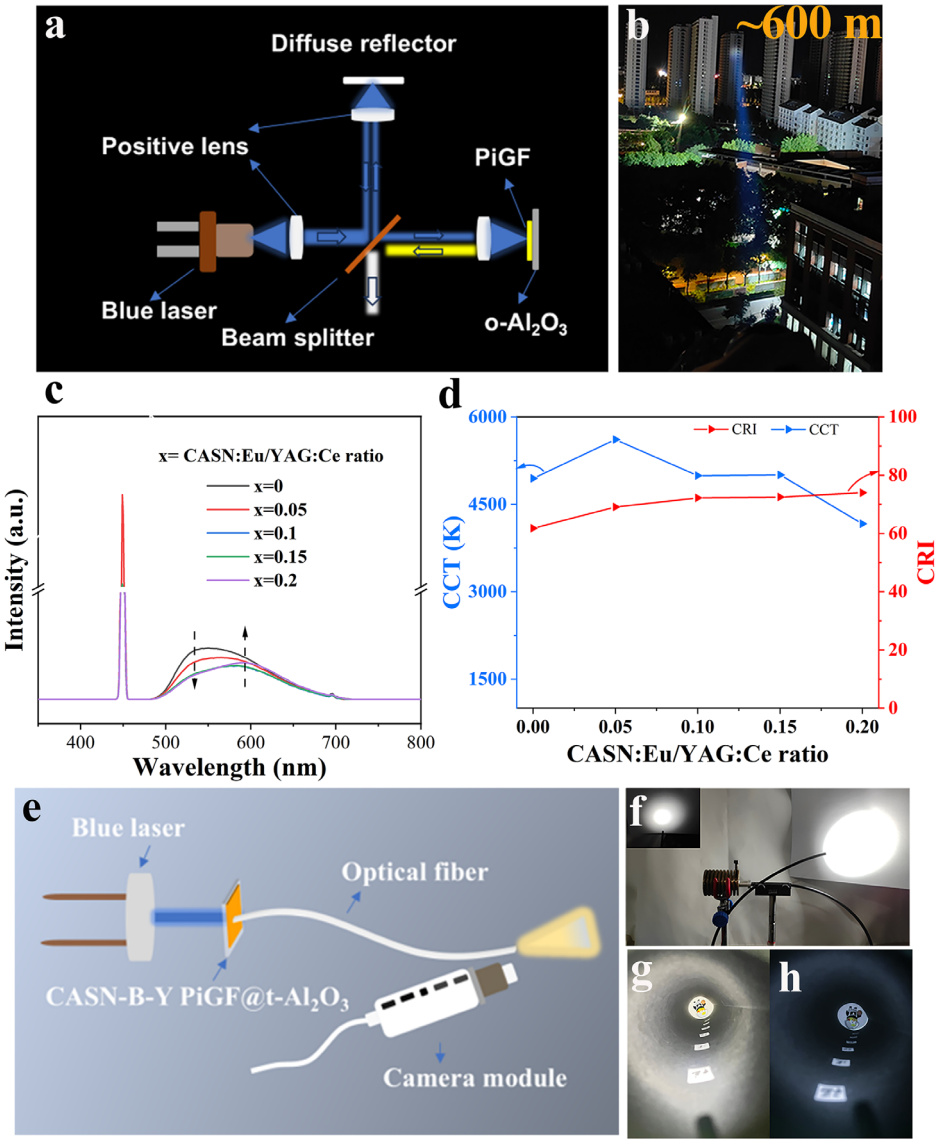

Figure 6. a) Schematic illustration of the laser-driven lighting configuration and light path in the reflective excitation mode; b) Illumination effect of the constructed laser-driven lighting source utilizing B-Y PiGF@o-Al_2O_3 as the color converter, demonstrating high brightness and long-range illumination at night; c) EL spectra and d) CCT & CRI of CASN-B-Y PiGF@t-Al_2O_3 at different CASN/YAG mass ratios; e) Schematic representation and f) photograph of the laser-driven miniature endoscope; Illumination comparison between endoscopes featuring g) B-Y PiGF-based and h) Y PiGF-based light sources.

that the limitations of this endoscope's construction arise primarily from the poor collimation of the LED light source. Clearly, the selection of the lighting source itself is also a critical factor in this regard. Furthermore, the comparison between endoscopes featuring B-Y PiGF-based and Y PiGF-based light sources demonstrates that the B-Y PiGF-based endoscope exhibits superior brightness and more uniform white light compared to the Y PiGF-based counterpart, underscoring the advantages of incorporating h-BN (Figure 6g,h).

3. Conclusion

In this work, we developed high-performance B-Y PiGF@o/t-Al_2O_3, achieving notable advancements in optical properties. The saturation threshold and LF of optimized B-Y PiGF@ o-Al_2O_3, in reflective excitation mode, reached a 95 % and 41 % improvement over the non-h-BN samples, respectively. This improvement was attributed to the efficient microzone heat conduction network formed by the h-BN particles (150 nm), which enhanced thermal dissipation and minimized thermal quenching, maintaining over 58 % of the luminescent intensity at 300 °C. In transmissive excitation mode, the incorporation of h-BN-induced pores in PiGF significantly enhanced the uniformity of the white light output, effectively eliminating the "yellow ring" effect. The B-Y PiGF@ t-Al_2O_3 exhibited precise tunability of CCT from 3810 to 8082 K and CRI from 63.3 to 74.0 by adjusting the weight ratio (YtG), film thickness, and incorporating CASN. Correspondingly, the developed composites exhibited the potential for

broader applications in fields requiring high-luminous-flux and thermally robust lighting sources, such as automotive lighting and medical endoscopy. Evidently, the development of thermally robust composite phosphor-in-glass film for laser-driven lighting aims to achieve high overall optical performance, paving the way for advancements in lighting technologies.

4. Experimental Section

Materials: The raw materials used in this study, including $Y_3Al_5O_{12}$: Ce^{3+} (YAG: Ce^{3+}, Beijing Grirem Advanced Materials Co., Ltd., China), $CaAlSiN_3$: Eu^{2+} (CASN: Eu^{2+}, Beijing Grirem Advanced Materials Co., Ltd., China), and h-BN (Shanghai Macklin Biochemical Technology Co., Ltd., China), were commercially sourced. The organic slurry was prepared by blending 2.5 mL ethyl acetate (Macklin, 99.8%), 1 mL terpineol (Aladdin, 95%), and 0.3 g ethyl cellulose (Aladdin, 98%) at 30 °C for 3 h at 600 rpm min^{-1}. The glass frits ($25SiO_2$-$30B_2O_3$-32ZnO-$4Al_2O_3$-$3K_2O$-$11Na_2O$-2.5CaO-$2BaCO_3$-1.5MgO, mol%) were produced using melt-quenching route. The stoichiometric chemicals (about 12 g, AR, Aladdin, China) were ground thoroughly and then melted in a muffle furnace (KSL-1700X, Hefei Kejing Materials Technology Co., Ltd., China) at 1350 °C for 2.5 h under ambient atmosphere. The glass melt was poured into a pre-heated brass mold (350 °C) quickly to obtain glass. Sapphire ($10 \times 10 \times 0.3$ mm, Crystal-Optech, China) and o-Al_2O_3 ($14 \times 19 \times 2$ mm, Foshan Xinghongfei Electronic Technology Co., Ltd.) served as heat sink substrates. A screen with a mesh size of 80 and a printing area of 10×10 mm was used to control the film thickness.

Fabrication of the B-Y PiGF: The preparation process for the B-Y PiGFs with innovative architecture is illustrated in Figure S1 (Supporting Information). First, h-BN powders were dispersed in an organic solvent and stirred for 10 min to ensure uniform dispersion. YAG: Ce^{3+} phosphor and glass frit were then mixed in a weight ratio of 3:5, and the mixture was thoroughly ground into fine powders. These powders were subsequently added to the h-BN suspension, and the resulting slurry was magnetically stirred at 600 rpm min^{-1} for 3 h (ZNCL-TS50ML, Shanghai Yushen Instrument Co., Ltd, China) to achieve a homogeneous mixture. The prepared slurry was blade-coated onto opaque Al_2O_3/transparent Al_2O_3 (o/t-Al_2O_3) substrates using a screen-printing technique. To control the thickness of the films accurately, a layer-by-layer deposition approach was employed. After each layer was printed, the film was heated on a hot plate (DLAB HP550-S, Dragon Laboratory Instruments Co., Ltd., China) at 120 °C for 10 min to solidify the layer before proceeding with subsequent printing steps. After the screen printing was complete, the PiGF films underwent a two-stage heat treatment in a muffle furnace. The first stage involved heating at 150 °C for 3 h to remove the organic solvent and binders (KSL-1100X, Hefei Kejing Materials Technology Co., Ltd., China). In the second stage, the temperature was increased to 640 °C and maintained for 30 min, ensuring that the glass matrix fully encapsulated the phosphor particles and h-BN (KSL-1100X, Hefei Kejing Materials Technology Co., Ltd., China). Samples were fabricated with h-BN weight fractions of 0 %, 2 %, 4 %, 6 %, 8 %, and 10 %, with film thicknesses controlled by varying the number of printed layers (1, 2, 3, 4, and 5 layers). For each combination of h-BN concentration and layer number, four samples were prepared to ensure reproducibility and reliability of the results. This systematic approach allowed for the evaluation of the effects of h-BN concentration and film thickness on the performance of PiGF materials.

Characterization: X-ray diffraction (XRD) analysis was performed to identify the crystalline phase structures of the DPs using a Rigaku SmartLab SE X-ray powder diffractometer with Cu Kα radiation operating at 40 kV. The microstructure and elemental distribution of the fabricated laser phosphors were examined using field emission scanning electron microscopy (SEM, SU8010, Hitachi, Japan) coupled with energy-dispersive X-ray spectroscopy (EDS, X-MaxN, Oxford Instruments, UK). Photoluminescence excitation (PLE), photoluminescence (PL) spectra, fluorescence lifetime, and temperature-dependent PL spectra were measured with a fluorescence spectrometer (FLS 1000, Edinburgh Instruments). Photoluminescence quantum yield (PLQY) was assessed by placing the sample inside a 15 cm barium sulfate-coated integrating sphere attached to the spectrophotometer. Correspondingly, the internal quantum efficiency (IQE) of all samples was determined using a fluorescence spectrometer (FLS1000) in combination with a 15 cm diameter integrating sphere. The external quantum efficiency (EQE) can be expressed as $\eta EQE = \eta Abs \times \eta IQE$, where ηIQE is measured directly, and ηAbs is calculated by evaluating the efficiency of absorbed blue light. Fluorescence images were captured using an optical microscope (Nikon, Eclipse, Ti2) combined with the FLS 1000. Surface temperatures were recorded using an infrared thermal imaging camera (TiS75, FLUKE), positioned 20 cm from the sample with its focus adjusted. The optical properties of the samples under laser excitation, including luminous spectra, luminous flux (LF), luminous efficacy (LE), correlated color temperature (CCT), color rendering index (CRI), and chromaticity coordinates, were measured in reflection mode using a system comprising an integrating sphere (30 cm in diameter, Labsphere, Inc.), a blue laser source (LSR445CP-FC-40 W, Lasever), and a CCD spectrometer (HR4000, Ocean Optics) (Figure S6, Supporting Information). The irradiated laser spot was adjusted using a lens system to a circular diameter of 1.8 mm, corresponding to an area of 2.54 mm^2.

Supporting Information

Supporting Information is available from the Wiley Online Library or from the author.

Acknowledgements

This research was supported by the National Natural Science Foundation of China (12304442, 52272141, 51972060, 12074068, 52102159, and 22103013), and Natural Science Foundation of Fujian Province (2024J02014, 2022J05091, 2021J06021, and 2021J01190).

Conflict of Interest

The authors declare no conflict of interest.

Author Contributions

Z.Z.Y., S.Z., and S.F.Z. contributed equally to this work. Z.Z.Y. and S.Z. synthesized the material and wrote the first draft. S.F.Z. made a significant contribution to the revision of the manuscript. S.S.L. and D.Q.C. helped them to analyze the experimental results and finish the final manuscript. J.W. and P.L. provided constructive suggestions to data analyses. T.P., L.W.Z., and F.H. helped to measure the spectroscopy. D.Q.C. supervised the project.

Data Availability Statement

The data that support the findings of this study are available from the corresponding author upon reasonable request.

Keywords

glass ceramics, laser-driven lighting, phosphor-in-glass, $Y_3Al_5O_{12}$: Ce^{3+}

Received: October 28, 2024
Revised: January 23, 2025
Published online:

[1] S. X. Li, L. Wang, N. Hirosaki, R.-J. Xie, *Laser Photonics Rev.* **2018**, *12*, 1800173.
[2] J. Cho, E. F. Schubert, J. K. Kim, *Laser Photonics Rev.* **2013**, *7*, 408.
[3] J. Cho, J. H. Park, J. K. Kim, E. F. Schubert, *Laser Photonics Rev.* **2017**, *11*, 1600147.
[4] C. Y. Ma, Y. G. Cao, *Appl. Phys. Lett.* **2021**,*118*, 210503.
[5] P. Zheng, S. X. Li, T. Takeda, J. Xu, K. Takahashi, R. D. Tian, R. Wei, L. Wang, T.-L. Zhou, N. Hirosaki, R.-J. Xie, *Acta Mater.* **2021**, *209*, 116813.
[6] Q. Li, W. G. Xiao, D. Zhang, D. D. Wang, G. J. Zheng, J. R. Qiu, *Laser Photonics Rev.* **2022**, *16*, 2200553.
[7] Z. K. Yu, J. Z. Zhao, Z. Z. Yang, Y. Mou, H. J. Zhang, R. P. Xu, Q. Wang, L. W. Zeng, L. Lei, S. S. Lin, H. Li, Y. Peng, D. Q. Chen, M. X. Chen, *Adv. Mater.* **2024**, *36*, 2406147.
[8] W. B. Chen, Y. Z. Wang, J. Xu, X. R. Chen, O. B. Jensen, Q. Y. Zhang, Z. G. Xia, *Laser Photonics Rev.* **2023**, *18*, 2300963.
[9] Y. J. Wang, Y. Y. Zhou, H. Ming, E. H. Song, C. Zhang, W. Y. Tang, Q. Y. Zhang, *Laser Photonics Rev.* **2023**, *17*, 2300012.
[10] Y. Q. Zhang, J. M. Liu, Y. J. Zhang, H. S. Yang, Y. X. Yu, Q. Y. He, X. J. Liang, Y. F. Liu, W. D. Xiang, *J. Rare Earths* **2022**, *40*, 717.
[11] Y. Y. Zhou, C. K. Yu, E. H. Song, Y. J. Wang, H. Ming, Z. G. Xia, Q. Y. Zhang, *Adv. Optical Mater.* **2020**, *8*, 2000976.
[12] G. Y. Xi, Z. Z. Zhou, J. Li, L. W. Zeng, S. S. Lin, P. F. Wang, H. Lin, Y. S. Wang, S. Zhou, F. Huang, G. L. Chen, D. Q. Chen, *Adv. Funct. Mater.* **2024**, *34*, 2401026.
[13] Z. Y. Yang, T. Boer, P. M. Braun, B. B. Su, Q. Y. Zhang, A. Moewes, Z. G. Xia, *Adv. Mater.* **2023**, *27*, 2301837.
[14] H. J. Wu, H. Wu, G.-H. Pan, L. L. Zhang, Z. D. Hao, J. H. Zhang, *J. Adv. Ceram.* **2023**, *12*, 1731.
[15] P. Huang, B. Y. Zhou, Q. Zheng, Y. Tian, M. M. Wang, L. J. Wang, J. L. Li, W. Jiang, *Adv. Mater.* **2020**, *32*, 1905951.
[16] Q. Yao, P. Hu, P. Sun, M. Liu, R. Dong, K. F. Chao, Y. F. Liu, J. Jiang, H. C. Jiang, *Adv. Mater.* **2020**, *32*, 1907888.
[17] X. J. Zhang, S. C. Si, J. B. Yu, Z. J. Wang, R. H. Zhang, B. F. Lei, Y. L. Liu, J. L. Zhuang, C. F. Hu, Y. J. Cho, R.-J. Xie, H.-W. Zhang, Z. F. Tian, J. Wang, *J. Mater. Chem. C* **2019**, *7*, 354.
[18] Y. Y. Liang, Y. J. Zhang, H. S. Yang, Y. Q. Zhang, J. D. Zhang, L. S. Wang, X. J. Liang, J. S. Zhong, W. D. Xiang, *Appl. Phys. Lett.* **2021**,*119*, 033303.
[19] P. Zheng, S. X. Li, R. Wei, L. Wang, T.-L. Zhou, Y.-R. Xu, T. Takeda, N. Hirosaki, R.-J. Xie, *Laser Photonics Rev.* **2019**, *13*, 1900147.
[20] Y. S. Sun, Y. Z. Wang, W. B. Chen, Q. Q. Jiang, D. D. Chen, G. P. Dong, Z. G. Xia, *Nat. Commun.* **2024**, *15*, 1033.
[21] S. Y. Bao, Y. Y. Liang, L. S. Wang, L. H. Wang, L. Xu, Y. Wang, X. J. Liang, W. D. Xiang, *ACS Sustainable Chem. Eng.* **2022**, *10*, 8105.
[22] G.-J. Wang, Q.-Q. Zhu, S.-J. Nie, Y. Zhai, S.-Q. Fang, J. Kang, L. Wang, *Laser Photonics Rev.* **2024**, *18*, 2301263.
[23] Q. X. Wen, Y. Wang, C. Zhao, L. Xu, X. D. Wang, Y. S. Xu, S. Lin, X. J. Liang, J. P. Liu, W. D. Xiang, *Laser Photonics Rev.* **2023**, *17*, 2200909.
[24] P. Sui, H. Lin, Y. Lin, S. S. Lin, J. J. Huang, J. Xu, Y. Cheng, Y. S. Wang, *Opt. Lett.* **2022**, *47*, 3455.
[25] C. Zhao, Q. X. Wen, S. Y. Bao, S. Pan, W. D. Xiang, X. J. Liang, *ACS Sustainable Chem. Eng.* **2023**, *11*, 12704.
[26] S. S. Lin, H. Lin, Q. M. Huang, H. Y. Yang, B. Wang, P. F. Wang, P. Sui, J. Xu, Y. Cheng, Y. S. Wang, *Laser Photonics Rev.* **2022**, *16*, 2200523.
[27] Q. G. Huang, H. Lin, B. Wang, S. S. Lin, P. F. Wang, P. Sui, J. Xu, Y. Cheng, Y. S. Wang, *J. Adv. Ceram.* **2022**, *11*, 862.
[28] X. M. Yue, J. Xu, H. Lin, S. S. Lin, R. F. Li, B. Wang, Q. G. Huang, P. F. Wang, P. Sui, Y. Cheng, Y. S. Wang, *Laser Photonics Rev.* **2021**, *15*, 2100317.
[29] S. X. Li, L. H. Huang, Y. Q. Guo, L. Wang, R.-J. Xie, *Mater. Horiz.* **2023**, *10*, 4581.
[30] S. X. Liao, S. L. Jin, T. Pang, S. S. Lin, Y. H. Zheng, R. H. Chen, G. Y. Xi, X. Y. Li, B. Zhuang, F. Huang, D. Q. Chen, *Adv. Funct. Mater.* **2024**, *34*, 2307761.
[31] L. Xu, X. D. Wang, L. H. Wang, S. Y. Bao, Y. Wang, X. J. Liang, W. D. Xiang, *ACS Sustainable Chem. Eng.* **2022**, *10*, 12817.
[32] Z. Z. Yang, S. Zheng, G. Y. Xi, T. Pang, S. X. Wang, Q. Y. Ye, B. Zhuang, D. Q. Chen, *J. Adv. Ceram.* **2023**, *12*, 2075.
[33] Z. Z. Yang, S. Zheng, T. Pang, S. X. Liao, J. W. Zhu, J. D. Lin, F. Huang, Y. H. Zheng, D. Q. Chen, *Adv. Mater. Technol.* **2023**, *8*, 2300132.
[34] H. Wang, Y. Mou, Y. Peng, Y. Zhang, A. G. Wang, L. L. Xu, H. L. Long, M. X. Chen, J. N. Dai, C. Q. Chen, *J. Alloys Compd.* **2020**, *814*, 152321.
[35] Y. Mou, Z. K. Yu, Z. Y. Lei, M. X. Chen, Y. Peng, *J. Alloys Compd.* **2022**, *918*, 165637.
[36] J. Y. Zhu, F. Li, Y. Z. Hou, H. Li, D. X. Xu, J. Y. Tan, J. H. Du, S. G. Wang, Z. B. Liu, H. A. Wu, F. C. Wang, Y. Su, H.-M. Cheng, *Nat. Mater.* **2024**, *23*, 604.
[37] B. Xie, H. C. Liu, R. Hu, C. F. Wang, J. J. Hao, K. Wang, X. B. Luo, *Adv. Funct. Mater.* **2018**, *28*, 1801407.
[38] A. Gurijala, R. B. Zando, J. L. Faust, J. R. Barber, L. Zhang, R. M. Erb, *Matter* **2020**, *2*, 1015.
[39] L. H. Wang, J. W. Liu, L. Xu, S. Y. Bao, Y. Wang, J. D. Zhang, X. J. Liang, W. D. Xiang, *Laser Photonics Rev.* **2023**, *17*, 2200585.
[40] T. L. Deng, L. H. Huang, S. X. Li, Q. Q. Zhu, L. Wang, T. Takeda, N. Hirosaki, R.-J. Xie, *Laser Photonics Rev.* **2022**, *16*, 2100722.